Nanoscale

PAPER

# Epitaxial nucleation of CVD bilayer graphene on copper

Yenan Song[a], Jianing Zhuang[b], Meng Song[c], Shaoqian Yin[a], Yu Cheng[a], Xuewei Zhang[a], Miao Wang[c], Rong Xiang[d], Yang Xia[e], Shigeo Maruyama[d], Pei Zhao*[a], Feng Ding*[b], and Hongtao Wang*[a]

Received 00th January 20xx,
Accepted 00th January 20xx

DOI: 10.1039/x0xx00000x

www.rsc.org/

Bilayer graphene (BLG) has emerged to be a promising candidate for the next-generation electronic applications especially when it exists in the Bernal-stacked form, but its large-scale production remains a challenge. Here we present an experimental and first-principles calculation study of the epitaxial chemical vapor deposition (CVD) nucleation process for Bernal-stacked BLG growth on Cu using ethanol as the precursor. Results show that a carefully adjusted flow rate of ethanol can yield a uniform BLG film with a surface coverage of nearly 90% and Bernal-stacking ratio of nearly 100% on ordinary flat Cu substrates, and its epitaxial nucleation of the second layer is mainly due to the active $CH_3$ radicals with the presence of a monolayer-graphene-covered Cu surface. We believe that this nucleation mechanism will help clarify the formation of BLG by epitaxial CVD process, and lead to many new strategies for scalable synthesis of graphene with more controllable structures and number of layers.

## Introduction

Bilayer graphene (BLG), a two-dimensional material consisting of two atomic layers of carbon honeycomb lattice, has emerged to be a promising candidate for the next-generation electronic applications especially when it exists in the Bernal- (AB-) stacked form, due to the fact that a bandgap of ~250 meV can be developed near its Dirac points by applying a vertical electric field across the two layers.[1, 2] However, by far the large-scale production of Bernal-stacked bilayer graphene remains a challenge. Although in the past years there have been many exciting achievements in the synthesis of large-size and high-quality monolayer graphene (MLG) using chemical vapor deposition (CVD) method on Cu substrates,[3-5] developing a practical and scalable method to obtain Bernal-stacked BLG is still a hot pursuit for future applications.

Previous reports have shown that the CVD synthesis of BLG on Cu is possible if more active carbon precursors or designed CVD process are adopted,[6-15] and the key point of these modification to ordinary CVD is to overcome the self-limiting nature of MLG on Cu. Usually, the second layer of BLG grows underneath the first-grown layer with shared nucleation sites, especially when methane is used as the carbon precursor, as evidenced from the isotope-labeling results,[10, 11] therefore the growth of these second nuclei will be strongly restricted and stopped by the expansion of their covered first layer. Moreover, because the nucleation of graphene grains is a super-saturation process of carbon on defective Cu surface, BLG growth from below also suggests a possible non-Bernal-stacking between the two graphene layers.[11] On the other hand, several reports also demonstrated a layer-by-layer epitaxial growth of BLG by CVD,[12-15] which has gradually become a topic of significant interest. Epitaxial CVD growth can yield relatively more uniform BLG with a high surface coverage and Bernal-stacking ratio, usually nearly 100%. During this growth, the second graphene layer grows on top of the first layer, and it is generally believed that the van der Waals (vdWs) force plays an important role in forming this high Bernal-stacking ratio.[13-15] However, many crucial aspects of the epitaxial CVD growth of BLG are still not fully understood and require additional investigation, during which the most important and fundamental one is the nucleation process of the second graphene layer on the formed first layer, *i.e.*, how the new graphene layer nucleate on top on the formed graphene when absent from the direct contact with the catalytic Cu surface.

To this end, we present an experimental and first-principles calculation study of the epitaxial CVD nucleation process for Bernal-stacked BLG growth on Cu using ethanol as the precursor. Results show that a carefully adjusted flow rate of ethanol can yield a uniform BLG film with a surface coverage of nearly 90% and Bernal-stacking ratio of nearly 100% on ordinary flat Cu substrates, and its epitaxial nucleation of the second layer is mainly due to the active $CH_3$ radicals with the presence of a MLG-covered Cu surface. We believe that this nucleation mechanism will help clarify the formation of BLG by epitaxial CVD process, and lead to many new strategies for scalable synthesis of graphene with more controllable structures and number of layers.

[a] Institute of Applied Mechanics and Key Laboratory of Soft Machines and Smart Devices of Zhejiang Province, Zhejiang University, Hangzhou 310012, P. R. China. Email: peizhao@zju.edu.cn; htw@zju.edu.cn.
[b] Institute of Textiles and Clothing, Hong Kong Polytechnic University, Kowloon, Hong Kong, China. Email: feng.ding@polyu.edu.hk.
[c] Department of Physics, Zhejiang University, Hangzhou 310012, P. R. China.
[d] Department of Mechnical Engineering, The University of Tokyo, Bunkyo-ku, Tokyo 113-8656, Japan.
[e] Institute of Microelectronics, Chinese Academy of Science, Beijing 100029, P. R. China.

† Electronic Supplementary Information (ESI) available: [Supplementary Figures]. See DOI: 10.1039/x0xx00000x

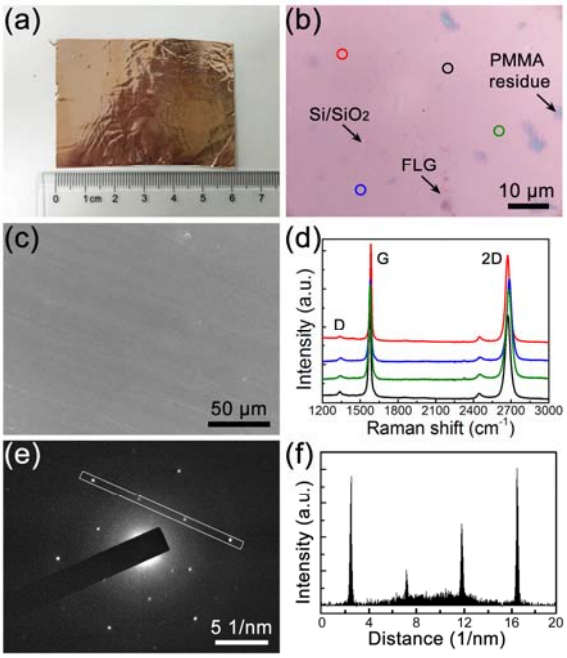


Fig. 1 (a) Photograph of a Cu foil after the CVD growth of BLG under the optimal condition for 3 hours. (b) OM image of a BLG film on a Si substrate with a 300-nm $SiO_2$ layer. (c) SEM image of as-grown BLG film on a Cu foil. (d) Typical Raman spectra of BLG measured from four random spots in (b). (e) SAED pattern of a BLG domain, which shows clear 6-fold symmetry. (f) Spot intensities in the white box in (e).

## Results and discussion

Zhao *et al.* has previously reported that the growth of Bernal-stacked BLG is an equilibrium process using ethanol as the carbon precusor,[15] but they used a folded Cu enclosure as the growth substrate, and uniform BLG was only obtained on the inside enclosure surface. This special substrate structure makes it difficult not only for the scaling-up synthesis, but also for the understanding of more detailed growth mechanism. In our approach, we chose the ethanol-based CVD system to grow BLG but attempted to reproduce its results on flat Cu, which as we show later will largely help understand its nucleation mechanism. Moreover, a flat Cu foil significantly enlarges the size of BLG films that can be grown in the CVD furnace when it is rolled up into a cylinder. As shown in the schematic image of the CVD system in Fig. S1 in Electronic Supplementary Information (ESI), we used the release valve of Ar gas to control its pressure to 0.5 atm. On the other hand, the ethanol tank was maintained at 19 ℃, which resulted in a saturated vapor pressure of 0.53 kPa for ethanol. Therefore, the pressure ratio between Ar and ethanol was approximately 10:1, and this ratio provided us the detailed ethanol partial pressures that were used in the CVD experiments. Moreover, Ar also behaves as the carrying and diluting gas for ethanol in the experiments. The uniform and scalable BLG films was obtained on flat Cu foils under the optimal condition (20 sccm Ar/ethanol, 3 hour growth, partial pressure of ethanol is ~3 Pa), as shown in **Fig. 1**a. Fig. 1b shows a typical optical microscopy (OM) image of the BLG film after transferred onto a Si substrate with a 300-nm $SiO_2$ layer, and the sample uniformity can be evaluated by its color contrast. No areas with different contrast are apparent, indicating that the layer number is uniform. The scanning electron microscope (SEM) image in Fig. 1c also demonstrates the uniformity of the as-grown graphene on the Cu foil. The layer number of the graphene film is conformed by Raman spectroscopy, as shown by the representative Raman spectra in Fig. 1d, which all show features of Bernal-stacked BLG such as a 2D-band (~2690 $cm^{-1}$) to G-band (~1582 $cm^{-1}$) intensity ratio ($I_{2D}/I_G$) of ~1, and an asymmetric 2D-band with a full-width at half-maximum (FWHM) value of ~45−60 $cm^{-1}$.[16] Fig. 1e shows the select area electron diffraction (SAED) pattern of a BLG domain using transmission electron microcopy (TEM), and only a single set of 6-fold symmetric diffraction spots is observed. The corresponding spot intensities in Fig. 1f clearly demonstrate the Bernal-stacking structure of these BLG samples.[16]

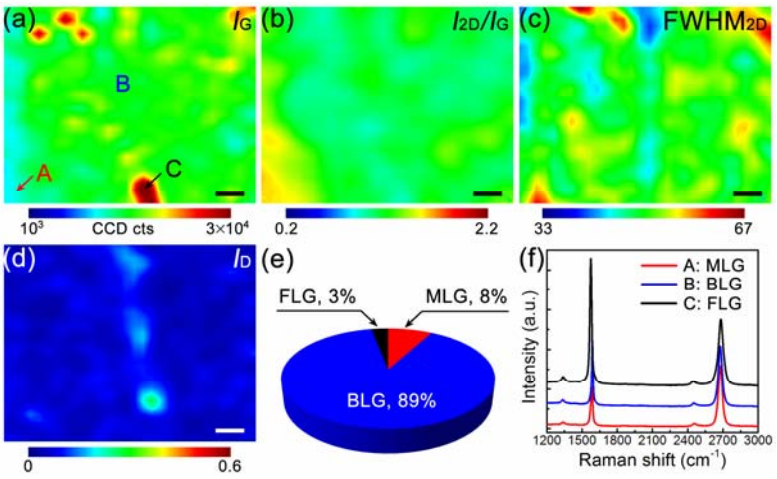


Fig. 2 Scanning Raman maps of ethanol-derived BLG on flat Cu for (a) $I_G$; (b) $I_{2D}/I_G$; (c) FWHM of the 2D-band; (d) $I_D/I_G$. Scale bars in (a−d): 10 μm. (e) Corresponding pie chart of graphene coverage for BLG, MLG, and FLG in the BLG film. (f) Raman spectra representative of MLG, BLG and FLG, measured from the regions indicated by red, blue, and black arrows in (a), respectively.

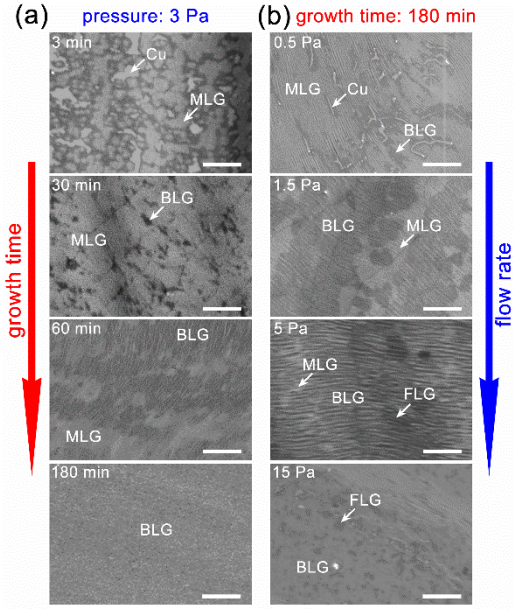


Fig. 3 (a) SEM images of BLG growth using a partial pressure of ethanol at 3 Pa with different growth periods of 3, 30, 60 and 180 min. (b) SEM images of graphene growth using different Ar/ethanol flow rates and the same growth time of 180 min, and the corresponding ethanol partial pressures are 0.5, 1.5, 5 and 15 Pa. Scale bars in (a) and (b): 5 μm.

The uniformity of these BLG samples can be further evaluated by the Raman contour maps of their $I_G$, $I_{2D}/I_G$, FWHM of 2D-band, and the D-band to G-band intensity ratio ($I_D/I_G$), as shown in **Fig. 2**a–d, respectively. These Raman spectra were collected over a 4500 μm$^2$ with 30×30 scanning points. We chose the range of Raman $I_{2D}/I_G$ from 0.7 to 1.3 and the FWHM of the 2D-band from 45 to 60 cm$^{-1}$ to evaluate Bernal-stacked BLG quality.[15, 17] The coverage of Bernal-stacked BLG, MLG and few-layer graphene (FLG) were determined to be ~89%, ~8% and ~3%, respectively, and no Raman features from twisted BLG were observed.[18] Fig. 2f shows the Raman spectra that are representative of MLG, BLG and FLG in BLG sample.

We interrupts the CVD process to obtain more information of the growth, by stopping the Ar/ethanol flow after different growth periods. The SEM images of these results are presented in **Fig. 3**a. The flow rate of Ar/ethanol is maintained as 20 sccm, and the corresponding partial pressure of ethanol is ~3 Pa. After 3 min, many MLG islands are found to nucleate on the Cu surface, with typical sizes smaller than 5 μm. Most of these islands coalesce to achieve a coverage of ~70% of the Cu surface. After 30 min, MLG completely forms and no unfilled gaps between islands are observed. The self-limiting growth stage of this MLG maintains for a short time and the nucleation of the second graphene layer starts soon. After 60 min, many new graphene islands appear and coalesce to form the second layer, with a total coverage of over 50% of the whole Cu/MLG surface. Moreover, it is visible that the graphene grain size of the secondly grown layer from ethanol is approximately 1 to 3 μm, significantly smaller than that from methane with equivalent pressure. The growth rate of the second layer is significantly reduced after 60 min and a continuous second layer finally completes after 3 hours and achieves an equilibrium state (Fig. S2 in ESI).

Ethanol can affect the BLG growth on a flat Cu in a more straightforward way, therefore it is necessary to investigate the relation between the ethanol flow and the yields, as shown in Fig. 3b. Apparently, a proper ethanol partial pressure is critical to obtain the best quality of BLG. When ethanol partial pressure is low, it yields MLG with unfilled gaps and randomly distributed BLG flakes, or non-uniform graphene film with discontinuous second layer. On the other hand, when ethanol partial pressure is high, graphene islands with more layers easily nucleate and expand, and finally yield a graphene film with more layers.

The previous BLG growth from ethanol has demonstrated that the growth follows a layer-by-layer epitaxy, in which the second layer growth atop of the first one.[15] Although it uses Cu envelopes other than flat Cu foils, we believe that this difference will not change this epitaxial growth mode. In the typical "growth-from-below" model, after the first graphene layer completes, the catalytically active Cu surface as well as the diffusion channels from the graphene grain edges to below the grains both disappear, making it prohibitive to expand the graphene layers that are below the first layer.[3] The epitaxial growth mode of BLG in our experiments can also be confirmed by its time-dependent SEM images in Fig.3, which clearly show that the grains of second graphene layer start to form after the full coalescence of the first layer, and keep expanding with prolonged CVD time.

To reveal the nucleation mechanism of the epitaxial CVD growth of BLG on Cu, we performed a theoretical study using first-principles calculations. The calculations is based on the fact that Cu surface can maintain its influence on graphene nucleation even after it is fully covered by a layer of graphene, evidential from the experimental results that no second graphene layers can be grown on transferred MLG/$SiO_2$/Si substrates at equivalent CVD environment (Fig. S3 in ESI). We use the basic forms of carbon radicals $CH_i$ ($i$ = 0, 1, 2, 3) as possible fundamental bricks for the nucleation of a new graphene layer, together with the Cu(111) surface and the formed graphene layer(s) as the studied system. More detailed geometries of these systems are shown in Fig. S4 in ESI. The relative binding strength of these $CH_i$ radicals on the Cu(111)/graphene surfaces can be presented in terms of their binding energy $E_b$

$$E_b = E_{sub} + E_{CHi} - E_{sys} \quad (1)$$

where $E_{sub}$, $E_{CHi}$, and $E_{sys}$ are the energies of the Cu(111)/graphene substrate, the $CH_i$ species, and the whole system, respectively. The total energy and binding energy data of $E_{sub}$, $E_{CHi}$, $E_{sys}$, and $E_b$ for these $CH_i$ on Cu(111)/graphene systems are summarized in Table S1 and Table S2 in ESI, respectively. During the nucleation process, a strong binding energy between the $CH_i$ species and substrate is needed. The calculation results demonstrate that the interactions between $CH_i$ and all Cu(111)/graphene substrates are in the forms of chemical bonding, as shown in **Fig. 4**. For MLG nucleation on Cu(111) surface, only radicals with a relatively stronger binding energy ($E_b$ > 3.0 eV) contribute to the growth of the first graphene layer, as mentioned in our previous report.[19] For BLG nucleation,

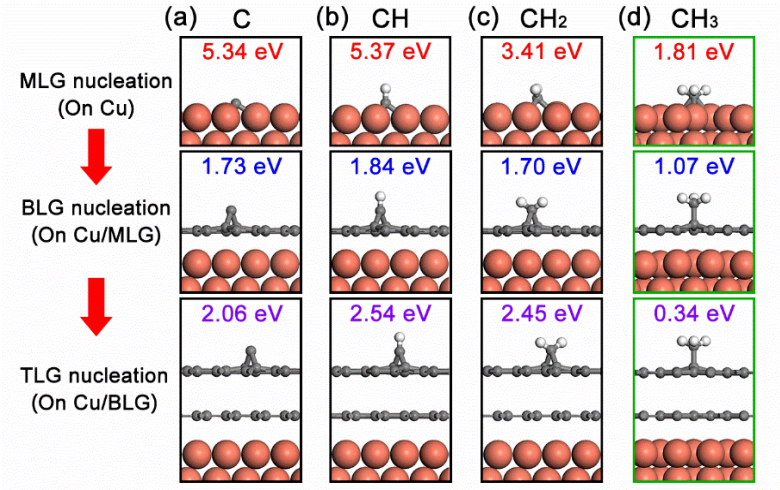


Fig. 4 Adsorption configurations and binding energies of (a) C monomer, (b) CH, (c) $CH_2$ and (d) $CH_3$ on top of the Cu surface, Cu surface with MLG, and Cu surface with BLG. Only the binding energies of $CH_3$ radicals are suitable for epitaxial nucleation of the second graphene layer.

radicals of C, CH and $CH_2$ all exhibit higher binding energies on Cu(111)/BLG than on Cu(111)/MLG (Fig. 4a−c), indicating that once a second graphene layer is nucleated, these radicals prefer to immediately nucleate a third layer on top of it. On the other hand, the $CH_3$ radicals have a binding energy of ~1.07 eV on Cu(111)/MLG and a binding energy of ~0.34 eV on Cu(111)/BLG (Fig. 4d), and this weakened binding strength makes it possible for the $CH_3$ radicals to be adsorbed on a Cu/MLG surface and nucleate only the second layer but not together with the third one. What the above calculations highlight is the binding energy differences for different radicals on different substrates, aiming to identify the most active radicals that facilitate the growth process. Moreover, since one radical is small in size compared to the defective sites that are capable of nucleation, such as the grain boundary, step or edge, we believe that the bonding behavior of radicals should be the similar as that on the flat substrate.

This scenario of $CH_3$-assisted nucleation is consistent with the reports by Wassei *et al*.[12] and Yan *et al*.[13], in which they both proposed that alkyl radicals is the main contribution to the epitaxial nucleation of a new graphene layer. This adsorption process of $CH_3$ radicals on the first graphene layer can also be assisted by a trapping mediated process,[20] in which a scattered $CH_3$ radical can be trapped at the basal plane of graphite surface for a short time at the environmental temperature much higher than its desorption temperature. This has been experimentally demonstrated by a Li-induced $CH_3Cl$ dissociative reaction with graphite.[21] We believe that this nucleation mechanism can also be further extended to other epitaxial CVD growth systems for BLG.

The above discussion is based on the assumption that the metal substrate is dominated by the Cu(111) facet. Theoretically, the top layer atomic packing on a Cu(111) facet owns a $C_{6v}$ symmetry,[22] the same as graphene and therefore allows a highly orientated graphene synthesis. In the above BLG growth experiments, most graphene first layer domains are in the six-fold symmetry and therefore we believe that the substrate is dominated by Cu(111) facets. Moreover, because we are considering the growth of the second graphene layer on the top of the first one, the effect of the type of Cu facet must be minor. Therefore, we believe the main conclusion of this study can also be applied to other Cu facets.

As to ethanol, its thermal decomposition at high temperatures are not well understood yet. Ethanol may decompose via many energetically accessible product channels. Considering the bond energies of C-O and C-C, the following two reactions

$$C_2H_5OH \rightarrow C_2H_4 + H_2O \quad (2)$$

$$\rightarrow CH_3 + CH_2OH \quad (3)$$

are expected to be the dominant channels.[23-28] Especially, channel reaction (3) is a barrierless path. We calculate the thermal decomposition products of ethanol at our equavalent experimental condition using the CHEMKIN-II software package, and show its time-dependent gas composition of ethanol in Fig. S5 in ESI. Approximately 97% of ethanol decomposes after 1 s, with various decomposition products of $C_2H_4$, $C_2H_2$, $CH_3$, $CH_2O$, etc. Considering that radicals are much more active in graphene growth reactions than molecules, among all types of radicals $CH_3$ show a molar fraction of ~0.26%, two and four orders of magnitute higher than those of $CH_2$ and CH, respectively, as shown in **Fig. 5**a. On the other hand, the thermal decomposition of methane is negligible at 1000 °C and can hardly generate any $CH_i$ radicals for graphene growth (molar fractions: $CH_3$ ~$10^{-8}$, $CH_2$ ~$10^{-17}$, CH ~$10^{-28}$). This is also consistent with the self-limiting growth behavior for MLG when methane is used.

For other alkanes that can also thermally decompose with $CH_3$ radicals such as $C_2H_6$, Wassei *et al*. has shown that BLG with a coverage of up to 49% can be obtained. Previous report has observed that graphene layers can form on HOPG by $CH_3$ radicals depending on the defects, and a largest sticking probabilities of $10^{-6}$ was observed when the HOPG surfaces are prestructured with nanometer sized etch pits.[29] Compared with $C_2H_6$, due to the decomposed products of $H_2$, $H_2O$, and/or other OH contained radicals, $C_2H_5OH$ induces etching and regrowth

 

sites in the firstly grown graphene layer,[15] which may also simultaneously behave as the more possible $CH_3$ nucleation sites. This increases the nucleation probability of the new graphene layer, and results in a higher coverage of BLG. Moreover, besides of generating $CH_3$ nucleation sites, the OH radicals also play an important role in accelerating the growth by lowering the energy barrier of carbon adatoms.[5]

We further consider the stability of each $CH_i$ radical on a Cu/MLG surface. Fig. 5b shows the relative Gibbs free energies of species of each $CH_i$ radical on Cu(111)/MLG as a function of the chemical potential of H ($\mu_H$). It is found that the stability of $CH_i$ highly depends on $\mu_H$, and $CH_3$ is the dominating species in the regime of $\mu_H > -1.24$ eV. In our experiments, no $H_2$ is used and $\mu_H$ mainly depends on the thermally decomposed H from ethanol. However, because the final decomposition products of ethanol usually react with H atoms,[25-28] H atoms can hardly be generated in all ethanol decomposition channels and its chemical potential is close to 0, which prefers the nucleation of the second graphene layer by $CH_3$ radicals.

Based on this, we propose the nucleation mechanism of ethanol-based epitaxial CVD growth for BLG on Cu in **Fig. 6**. For the MLG, ethanol behaves similarly as methane,[30] and the C, CH, $CH_2$ radicals catalyzed from ethanol by Cu contribute the most to its nucleation and growth. After the MLG formation, the absence of direct contact between ethanol and Cu makes it difficult to generate radicals of C, CH and $CH_2$, whose binding energies do not match the nuclation of only BLG as well. On the other hand, $CH_3$ radicals play a crucial role in nucleating the second graphene layer, not only because it is a product of thermally decomposed ethanol, but also because of its suitable binding energies on Cu/MLG and Cu/BLG.

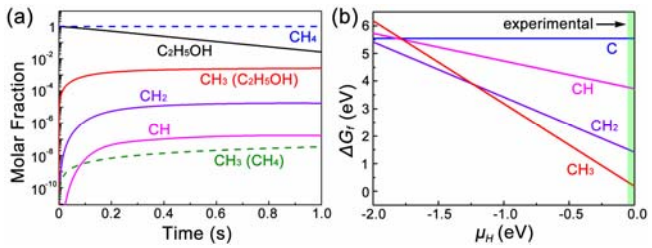


Fig. 5 (a) Decomposition products of $CH_i$ radicals from $C_2H_5OH$ and $CH_4$ at high temperature, calculated by CHEMKIN-II. (b) the relative Gibbs free energies of species of each CHi radical on Cu(111)/MLG as a function of the chemical potential of H.

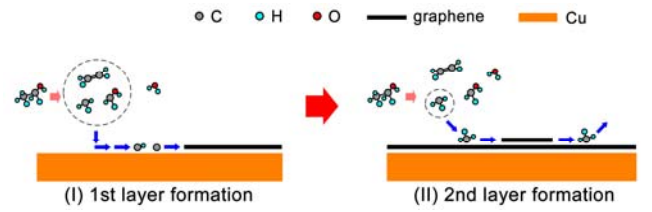


Fig. 6 Schematic of the possible mechanism for epitaxial CVD growth of BLG on Cu using ethanol as the carbon precursor.

Finally, it needs to be emphasized that after the grain nucleation of second graphene layer by $CH_3$ radicals, its followed carbon deposition process remains unclear. Although the C-H dissociation energy is calculated to be 480 kJ/mol,[31] which makes it impossible for the direct dissociation of another C-H bond in the nucleated $CH_3$ radical, the actual energy barrier for $CH_3$ and H exchange is considerably lower and accessible at reaction temperatures.[32] Moreover, the –OH radicals may also play some role in lowering the activation energy of the edge dehydrogenation, similar as that in an oxygen-assisted CVD growth for centimeter-scale graphene single crystals.[5]

## CONCLUSION

In conclusion, we demonstrate an experimental and first-principles calculation study of the epitaxial CVD growth for Bernal-stacked BLG on Cu using ethanol. The surface coverage of BLG in the sample is nearly 90% and Bernal-stacking ratio is nearly 100%. Under the equilibrium CVD environment, the BLG growth exhibits two self-limiting processes for the two graphene layers but with significantly different growth rates. First-principles calculation results show that the epitaxial nucleation of the second graphene layer is mainly due to the active $CH_3$ radicals and the Cu substrate with a covered graphene layer. We believe we have uncovered a new territory in the CVD nucleation mechanism of epitaxial graphene growth, and hope that this understanding will bring the advent of CVD graphene growth with more precise control of radicals forward.

## Experimental section

### BLG synthesis

BLG was synthesized by low-pressure CVD using bubbled ethanol. Commercially available Cu foils (25-μm-thick, #46365, Alfa Aesar China Chemical Co., Ltd.) were used as received. A flat Cu foil was placed into a hot-wall CVD quartz chamber (i.d.=60 mm), and annealed at 1000 ºC for 30 minutes with 100 sccm $H_2$, followed by introducing 20 sccm Ar/ethanol mixture gas. $H_2$ was stopped at the growth step of graphene. After growth, the chamber was slowly cooled to room temperature at a rate of 10–20 ºC $min^{-1}$.

### Graphene transfer

BLG film on copper was firstly coated with polymethyl methacrylate (PMMA, 4 wt% in anisole) by the spin-coating method, and baked on the hotplate at 140 ºC for 30 min. The graphene film on the back side of Cu foil was treated by an O2 plasma (100 W) for 30 s. The Cu substrate was then etched away in 1 M $FeCl_3$ solution and the PMMA/graphene film was rinsed in DI water for 3 times and transferred onto the Si substrate. Finally the PMMA layer was removed by a hot acetone.

### Characterizations

Characterizations of as-grown and transferred BLG were carried out by optical microscopy (Olympus BXFM-ILHS, Olympus Co., Ltd), scanning electron microscopy (SEM, 5 kV, S-3400,

Hitachi Co., Ltd.), confocal micro-Raman spectroscopy (LabRAM HR Evolution, Horiba Co., Ltd.), and transmission electron microscopy (JEM-2100, JEOL Co., Ltd.).

#### First-principles calculations

The first-principles calculations are performed with the density-functional theory approach as implemented by the Vienna ab initio Simulation Package (VASP)[33, 34]. The exchange-correlation energy is treated in the Perdew-Burke-Ernzerhof (PBE) version of the generalized-gradient approximation (GGA) functional[35, 36]. In order to accurately describe the vdWs between a $CH_i$ ($i$ = 0, 1, 2, 3) radical and Cu surface, the PBE functional with the vdWs correction (DFT-D3)[37] has also been used. The energy cutoff of the plane-wave expansion is set to 400 eV. All structures are optimized by the conjugate gradient method until the forces acting on each atom are less than 0.01 eV·Å−1. Cu(111) surfaces is modelled using slab geometry with four metal atomic layers in which the bottom-layer atoms are fixed at their respective bulk positions. For the geometry optimization, all atoms except for the fixed bottom-layer atoms are fully relaxed and then various $CH_i$ species are put on the metal substrate surface for further optimization.

#### Ethanol decomposition simulation

Simulation of ethanol decomposition was performed using SENKIN[38, 39], a computer program that predicts the time-dependent chemical-kinetic behaviour of a homogeneous gas mixture in a closed system. This has been incorporated into CHEMKIN-II[40], which is a package of computer codes for the analysis of gas-phase chemical kinetics. Constant-temperature and constant-pressure conditions were chosen for the calculations using temperatures and pressures that had been experimentally found to be optimum for BLG growth.

## Acknowledgements

The authors are grateful to Prof. Zhongfan Liu (Peking University, China) for his helpful discussions. Part of this work was financially supported by the National Science Foundation of China (11502231, 11321202, 11322219, 61471317), National Program for Special Support of Top-Notch Young Professionals, Zhejiang Provincial Natural Science Foundation of China (LQ15A020001) and the National Key Scientific Instruments and Equipment Development Project of China (61427901).

## References

1. Y. Zhang, T.-T. Tang, C. Girit, Z. Hao, M. C. Martin, A. Zettl, M. F. Crommie, Y. R. Shen and F. Wang, *Nature*, 2009, **459**, 820–823.
2. K. F. Mak, C. H. Lui, J. Shan and T. F. Heinz, *Phys. Rev. Lett.*, 2009, **102**, 256405.
3. X. S. Li, W. W. Cai, J. H. An, S. Kim, J. Nah, D. X. Yang, R. Piner, A. Velamakanni, I. Jung, E. Tutuc, S. K. Banerjee, L. Colombo and R. S. Ruoff, *Science*, 2009, **324**, 1312–1314.
4. S. Bae, H. Kim, Y. Lee, X. Xu, J.-S. Park, Y. Zheng, J. Balakrishnan, T. Lei, H. Ri Kim, Y. I. Song, Y.-J. Kim, K. S. Kim, B. Ozyilmaz, J.-H. Ahn, B. H. Hong and S. Iijima, *Nat. Nanotechnol.*, 2010, **5**, 574–578.
5. Y. Hao, M. S. Bharathi, L. Wang, Y. Liu, H. Chen, S. Nie, X. Wang, H. Chou, C. Tan, B. Fallahazad, H. Ramanarayan, C. W. Magnuson, E. Tutuc, B. I. Yakobson, K. F. McCarty, Y.-W. Zhang, P. Kim, J. Hone, L. Colombo and R. S. Ruoff, *Science*, 2013, **342**, 720–723.
6. S. Lee, K. Lee and Z. Zhong, Nano Lett., 2010, 10, 4702–707.
7. Z. Sun, A.-R. O. Raji, Y. Zhu, C. Xiang, Z. Yan, C. Kittrell, E. L. G. Samuel and J. M. Tour, *ACS Nano*, 2012, **6**, 9790–9796.
8. H. Zhou, W. J. Yu, L. Liu, R. Cheng, Y. Chen, X. Huang, Y. Liu, Y. Wang, Y. Huang and X. Duan, *Nat. Commun.*, 2013, **4**, 2096.
9. H.-B. Sun, J. Wu, Y. Han, J.-Y. Wang, F.-Q. Song and J.-G. Wan, *J. Phys. Chem. C*, 2014, **118**, 14655–14661.
10. Q. Li, H. Chou, J.-H. Zhong, J.-Y. Liu, A. Dolocan, J. Zhang, Y. Zhou, R. S. Ruoff, S. Chen and W. Cai, *Nano Lett.*, 2013, **13**, 486–490.
11. W. Fang, A. L. Hsu, R. Caudillo, Y. Song, A. G. Birdwell, E. Zakar, M. Kalbac, M. Dubey, T. Palacios, M. S. Dresselhaus, P. T. Araujo and J. Kong, *Nano Lett.*, 2013, **13**, 1541–1548.
12. J. K. Wassei, M. Mecklenburg, J. A. Torres, J. D. Fowler, B. C. Regan, R. B. Kaner and B. H. Weiller, *Small*, 2012, **8**, 1415–1422.
13. K. Yan, H. Peng, Y. Zhou, H. Li and Z. Liu, *Nano Lett.*, 2011, **11**, 1106–1110.
14. L. Liu, H. Zhou, R. Cheng, W. J. Yu, Y. Liu, Y. Chen, J. Shaw, X. Zhong, Y. Huang and X. Duan, *ACS Nano*, 2012, **6**, 8241–8249.
15. P. Zhao, S. Kim, X. Chen, E. Einarsson, M. Wang, Y. Song, H. Wang, S. Chiashi, R. Xiang and S. Maruyama, *ACS Nano*, 2014, **8**, 11631–11638.
16. L. M. Malard, M. A. Pimenta, G. Dresselhaus and M. S. Dresselhaus, *Phys. Rep*., 2009, **473**, 51–87.
17. Z. Peng, Z. Yan, Z. Sun and J. M. Tour, *ACS Nano*, 2011, **5**, 8241–8247.
18. Z. H. Ni, Y. Y. Wang, T. Yu, Y. M. You and Z. X. Shen, *Phys. Rev. B*, 2008, **77**, 235403.
19. H. Shu, X.-M. Tao and F. Ding, *Nanoscale*, 2015, **7**, 1627–1634.
20. C. T. Rettner, E. K. Schweizer, H. Stein, *J. Chem. Phys.*, 1990, **93**, 14442.
21. L. Mandeltort, P. Choudhury, J. K. Johnson and J. T. Yates, *J. Phys. Chem. Lett.*, 2012, **3**, 1680–1683.
22. A. H. Castro Neto, F. Guinea, N. M. R. Peres, K. S. Novoselov and A. K. Geim, *Rev. Mod. Phys.*, 2009, **81**, 109–162.
23. B. Hou, R. Xiang, T. Inoue, E. Einarsson, S. Chiashi, J. Shiomi, A. Miyoshi and S. Maruyama, *Jpn. J. Appl. Phys.*, 2011, **50**, 065101.
24. R. Xiang, B. Hou, E. Einarsson, P. Zhao, S. Harish, K. Morimoto, Y. Miyauchi, S. Chiashi, Z. Tang and S. Maruyama, *ACS Nano*, 2013, **7**, 3095–3103.
25. J. Park, R. S. Zhu and M. C. Lin, *J. Chem. Phys.*, 2002, **117**, 3224–3231.
26. J. Li, A. Kazakov and F. L. Dryer, *J. Phys. Chem. A*, 2004, **108**, 7671–7680.
27. R. Sivaramakrishnan, M. C. Su, J. V. Michael, S. J. Klippenstein, L. B. Harding and B. Ruscic, *J. Phys. Chem. A*, 2010, **114**, 9425–9439.
28. Z. F. Xu, K. Xu and M. C. Lin, *J. Phys. Chem. A*, 2011, **115**, 3509–3522.
29. R. Wellmann, A. Böttcher, M. Kappes, U. Kohl and H. Niehus, *Surf. Sci.*, 2003, **542**, 81–93.
30. P. Zhao, A. Kumamoto, S. Kim, X. Chen, B. Hou, S. Chiashi, E. Einarsson, Y. Ikuhara and S. Maruyama, *J. Phys. Chem. C*, 2013, **117**, 10755–10763.
31. K. May, S. Dapprich, F. Furche, B. V. Unterreiner, R. Ahlrichs, *Phys. Chem. Chem. Phys.* 2000, **2**, 5084.
32. L. K. Rutz, H. Bockhorn, J. W. Bozzelli, Abstracts of Papers of *The American Chemical Society* 2004, **227**, U1100–U1101.
33. P. E. Blöchl, *Phys. Rev. B*, 1994, **50**, 17953–17979.
34. G. Kresse and J. Furthmüller, *Phys. Rev. B*, 1996, **54**, 11169–11186.
35. J. P. Perdew, K. Burke and M. Ernzerhof, *Phys. Rev. Lett.*, 1996, **77**, 3865–3868.
36. G. Kresse and D. Joubert, *Phys. Rev. B*, 1999, **59**, 1758–1775.
37. S. Grimme, S. Ehrlich and L. Goerigk, *J. Comput. Chem.*, 2011, **32**, 1456–1465.

 

38. A. Varykhalov, J. Sanchez-Barriga, A. M. Shikin, C. Biswas, E. Vescovo, A. Rybkin, D. Marchenko and O. Rader, *Phys. Rev. Lett.*, 2008, **101**, 157601.
39. Y. Murata, V. Petrova, B. B. Kappes, A. Ebnonnasir, I. Petrov, Y. H. Xie, C. V. Ciobanu and S. Kodambaka, *ACS Nano*, 2010, **4**, 6509–6514.
40. R. Q. Zhao, Y. F. Zhang, T. Gao, Y. B. Gao, N. Liu, L. Fu and Z. F. Liu, *Nano Res.*, 2011, **4**, 712–721.